Proceedings of Global Power and Propulsion Society
ISSN-Nr: 2504-4400
GPPS Hong Kong 2023
October 17 - 19, 2023
www.gpps.global

GPPS-TC-2023-0163

STABILITY ANALYSIS OF THE N-BLADED SYSTEM WITH BLADE-TO-BLADE INTERACTION

Youngkuk Yoon
Seoul National University
truesky1218@snu.ac.kr
Seoul, South Korea

Seung Jin Song
Seoul National University
sjsong@snu.ac.kr
Seoul, South Korea

ABSTRACT

This paper presents a new approach based on simplified dynamic modelling of the blade and blade-to-blade interaction, which generally occurs due to flow structures with large extent such as tip clearance vortex. The model considers the blade-to-blade interaction as the primary cause of the local instability. By linearizing the blade-to-blade interaction, the stability of the system can be examined via eigenvalue analysis of the matrix differential system. Two- and three-bladed system are examined, and the results are qualitatively compared with the previous experimental results. Also, a graphical approach for investigating eigenvalues of general N-bladed system is given, and the behaviour of the system eigenvalues with varying model parameters are explained.

INTRODUCTION

Flow instabilities in turbomachinery cause unexpected vibration, whose frequency components are other than harmonics of shaft rotating frequency, to the system. These flow instabilities can be divided into two parts: global instability and local instability. Global instability which includes compressor surge is characterized as axial oscillation of the entire system, such as large oscillation of the flow rate. It was shown that the global instabilities are closely related to some "characteristic" lumped parameters of the corresponding turbomachinery. For compressor surge, the positive slope of the $\psi(\phi)$ curve has been shown to be responsible for the occurrence of the surge (Moore and Greitzer, 1986). Physically, if the slope of the characteristic curve is positive, small (positive) perturbation of the flow rate from the equilibrium point will increase the pressure ratio and further increase the downstream throttle flow rate which positively feeds-back the initial perturbation. Also, it was shown that the positive mass flow gain factor, $M \equiv \frac{\partial a}{\partial \alpha_1}$, where a is the normalized cavity volume and α_1 is the incidence angle, is the key factor for the cavitation surge, while small (positive) perturbation of the flow rate will be amplified due to decreasing cavity volume as incidence increases (Tsujimoto et al., 2001).

For the local instability, similar approaches have been taken to analytically investigate the instability using the lumped parameters which represent the characteristics of the whole flow passage. For example, it was shown that also for the rotating cavitation, positive mass flow gain factor is a dominant cause by using 2-D actuator disk model (Tsujimoto et al., 1993). Furthermore, other 2-D type methods have been developed to bypass the difficulty of experimental measurements of the lumped parameters. Watanabe et al. (1999) and Horiguchi et al. (2000) proposed a 2-D potential flow singularity method, combined with a closed cavity model, to perform the linear stability analysis under small perturbation and to predict local instabilities, including super-synchronous rotating cavitation and alternate blade cavitation. Semenov and Tsujimoto (2003) incorporated a viscous wake model into the 2-D potential flow model to obtain an analytical solution for the asymmetric cavitation.

However, in the turbopump inducer, it was experimentally shown that the local instabilities such as super-synchronous- and sub-synchronous rotating cavitation occurs only at the tip region of the impeller (Tsujimoto et al., 1997). For compressor, Vo et al. (2008) showed that spike-type rotating stall is triggered by the flow structure at the blade tip region. Also, Xu et al. (2021) performed a global stability analysis to show that the compressor flow field is the most unstable under disturbances confined at the blade tip region. Therefore, in such cases, if the fluid structure at the tip

does not vary much the lumped parameters concerning entire flow passage, previous 2-D actuator disk model might not well reflect the physical mechanism of the local instability. Thus, while it has been shown that the physical mechanism of the local instabilities is blade-to-blade interaction caused by the tip flow structure such as tip leakage flow (Kang et al., 2009; Hewkin-Smith et al., 2019; Kim et al., 2019), analytical model including the discrete blade-to-blade interaction should be separately constructed.

Hence, this paper proposes an analytical framework which can be used to investigate the local instabilities whose impacts are not so large on the lumped parameters. The present model focuses on the local instabilities of finite blade impellers, especially on two- and three-bladed impellers. The blades and their interaction are modelled in their simplest form with mass-spring-damper lattice with forced vibration due to the interaction which is linearized for the present model. It is shown that various local instabilities can be explained, including alternate blade cavitation on two-bladed inducer and super-synchronous rotating cavitation on three-bladed inducer, by concerning the blade-to-blade interaction as the only physical mechanism.

FINITE BLADE SYSTEM MODEL

In this analysis, the finite blade system is simplified as Fig. 1. First, it was assumed that the physical mechanism of the flow instability is blade-to-blade interaction, and it is manifested as a change in incidence due to some flow structure on the preceding blade (e.g., incidence increase due to tip leakage flow of the preceding blade, or incidence decrease due to collapse of the tip leakage vortex cavitation). If the preceding blade changes the incidence of the blade, the same flow structure on the blade will change and it will also affect the following blade by its on way. This succession of blade-to-blade interaction is the key mechanism of the instability propagation. Meanwhile, previous research including both analytical and experimental studies (von Kármán and Sears, 1938; Murayama et al., 2006) has showed that the aerodynamic response of the blade does not response to the incidence perturbation in quasi-steady manner, but it reacts with certain magnitude change and phase lag. Therefore, each blade is modelled with mass-spring-damper system, whose displacement corresponds to the incidence angle, to cover this dynamic characteristic. It should be noted that this representation is an approximation under small reduced frequency ($k \equiv \frac{2\pi f C}{U} < 1$) while in all frequency range, it is highly probable that the dynamic characteristic of the blade does not follow the simple mass-spring-damper system. In the present study, each blade is modelled with following equations, where $n = 1, \ldots, N$:

$$\dot{x_n} = [\dot{x_n}], \qquad (1)$$

$$\ddot{x_n} = \frac{1}{\mathrm{a}}\left(-b[\dot{x_n}] - [x_n] + \alpha_f + \Delta\alpha_{n-1,n}\right). \qquad (2)$$

$\Delta\alpha_{0,1}$ is defined as $\Delta\alpha_{N,1}$ due to the periodic structure of the N-bladed system. α_f is the incidence without any blade-to-blade interaction, which can be determined by the flow coefficient. $\Delta\alpha_{n-1,n}$ represents blade-to-blade interaction which can be generally considered as a function of x_{n-1}.

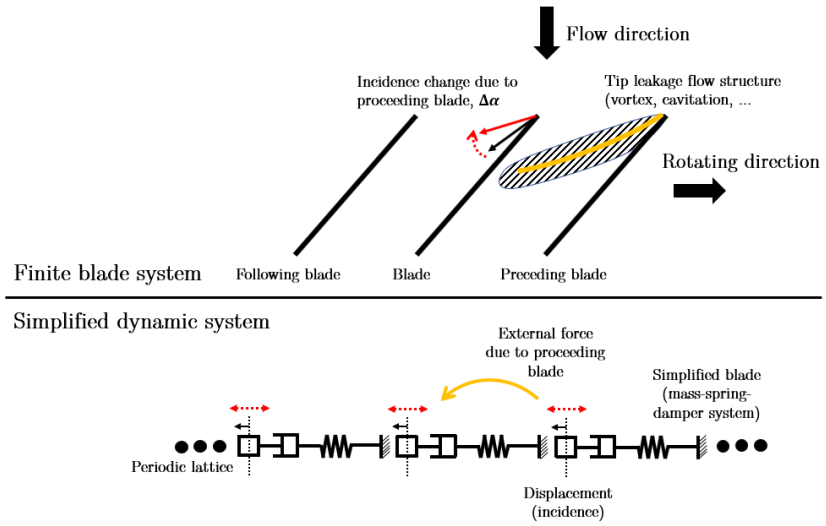

Figure 1 Schematic Diagram of the Blade Model

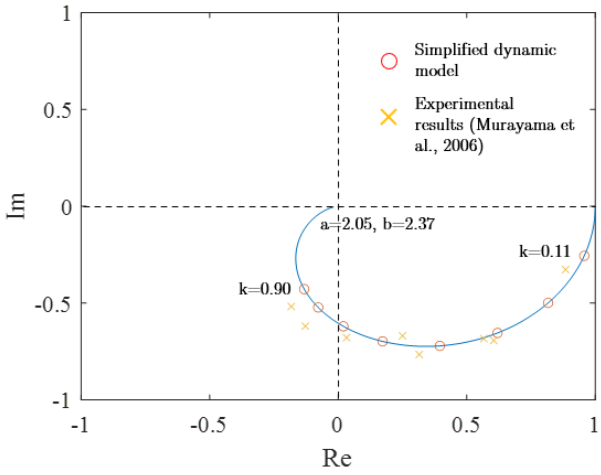

Figure 2 Unsteady Response of the Tip Leakage Vortex Cavitation

In actual turbomachinery, equivalent mass, a, and equivalent damping constant, b, can be obtained by experiments or numerical simulations which have been performed under periodic inlet flow. For example, under periodic incidence, the extent of the tip leakage vortex cavitation (TLVC) varies with significant phase and magnitude change compared with the quasi-steady case (Murayama et al., 2006). From the unsteady response of TLVC, effective incidence can be determined by comparing with the steady response of TLVC. Thus, for given input of periodic incidence, incidence output can be calculated, and Bode plot can be constructed. Fig. 2 shows such plot of both experimental and simplified unsteady response of the tip clearance vortex cavitation on a complex domain. By fitting the variables, a and b, the unsteady response of the system can be represented by a simplified mass-spring-damper system. Similarly, for different geometry or flow structure of specific turbomachinery of interest, equivalent mass and damping constant can be obtained by an experiment or CFD under periodic inlet condition. Nevertheless, to cover possible various frequency responses of the system, the present analysis examines wide range of a and b, rather than confining a and b to specific values.

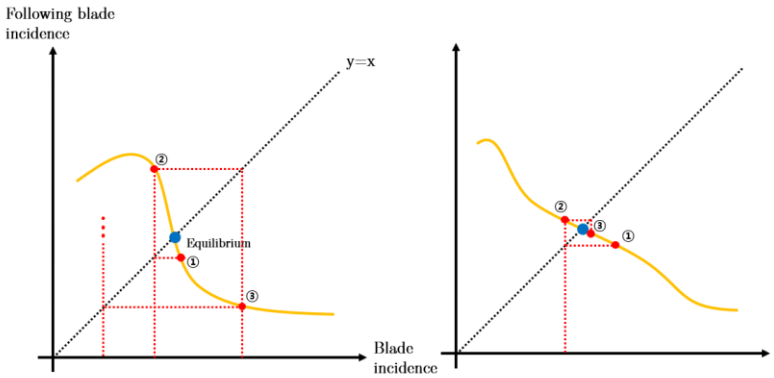

Figure 3 Schematic Diagram of the Blade-to-Blade Interaction

To further simplify the present analysis, quasi-steady behaviour of the given system is examined in Fig. 3. Fig. 3 shows the system in the spirit of the Poincaré recurrence map. The abscissa of the graph is the incidence angle of the present blade and the ordinate is the incidence angle of the following blade, which is determined by the flow coefficient and blade-to-blade interaction, $\alpha_f + \Delta\alpha_{n-1,n}$ (bold yellow line). If the system is in equilibrium, the system will stay on the intersection between $y = x$ line and the yellow line (blue point), while the present blade will induce the same incidence on the following blade, and that following blade will also induce the same incidence on the next following blade, and so on. However, the stability of this equilibrium point should be examined via inserting small perturbation to the system. For example, if the blade-to-blade interaction is given as right part of Fig. 3, small perturbation to position ① will induce position ② to the following blade (in a quasi-steady manner), and this position will successively induce position ③ to the next following blade, and hence we can conclude this equilibrium is unstable and will diverge (even though this divergence will be eventually limited by the non-linearity of the interaction). On the other hand, if the blade-to-blade interaction is given as left part of Fig. 3, with the same logic, the equilibrium is stable and small perturbation will eventually converge to the equilibrium point. From this analysis, it can be seen that the key dynamics which determines the stability of the equilibrium and enables the local instability to propagate is the slope of the blade-to-blade

interaction, which can be also validated by the Hartman-Grobman theorem. Thus, in the present analysis, only the slope of the interaction, $\partial(\alpha_f + \Delta\alpha_{n-1,n})/\partial(x_{n-1}) \equiv c$ is considered, and, instead of Eq. (2), following Eq. (3) is analysed:

$$\ddot{x_n} = \frac{1}{a}\left(-b[\dot{x_n}] - [x_n] + cx_{n-1}\right). \quad (3)$$

APPLICATION ON TWO-BLADED IMPELLER

The matrix differential equation of the two-bladed impeller is expressed as follows:

$$\dot{X} = \begin{bmatrix} 0 & 1 & 0 & 0 \\ -1/a & -b/a & c/a & 0 \\ 0 & 0 & 0 & 1 \\ c/a & 0 & -1/a & -b/a \end{bmatrix} \mathrm{X}, \quad (4)$$

where $\mathrm{X} = [\mathrm{x}_1\ \dot{x_1}\ \mathrm{x}_2\ \dot{x_2}]^T$.

Therefore, the characteristic equation of the given matrix is obtained as Eq. (5).

$$\frac{(a\lambda^2+b\lambda+1)^2-c^2}{a^2} = 0 \quad (5)$$

The eigenvalue of the system is as follows:

$$\lambda = \frac{-b\pm\sqrt{b^2-4ac-4a}}{2a} \ or \ \frac{-b\pm\sqrt{b^2+4ac-4a}}{2a} \quad (6)$$

To make the equilibrium point unstable, at least one of the eigenvalues should have real part larger than 0. To do so, the value inside the square root should be positive and furthermore, larger than b^2. Thus, only if $|c| > 1$, the instability will develop regardless of a and b. Two different cases can be identified under this condition: $c > 1$ and $c < -1$. Fig. 4 shows the graphical representation of both cases. If c is larger than 1, small perturbation will amplify and, in linear system, it will diverge indefinitely. However, in actual situation, the blade-to-blade interaction (yellow line) should again cross the line $y = x$ while it cannot reach to infinity, and the system will shift to the nearest stable equilibrium point or at least trapped in a limit cycle. Although the case $c > 1$ does not reveal any significant behaviour and additionally requires the behaviour of the near equilibrium point to fully describe the system, the case $c < -1$ shows an interesting situation. If c is smaller than -1, the incidence on one blade increases while it decreases on the other. Therefore, the local instability predicted by this behaviour is an asymmetric disturbance which is attached to the rotating frame. This instability is frequently observed in two-bladed turbopump inducer in the form of alternate blade cavitation (Huang et al., 1998). Under alternate blade cavitation, smaller tip leakage vortex cavitation is induced on one blade and larger one is developed on the other blade. From this analysis, it can be suspected that this instability is due to negative slope of the blade-to-blade interaction, and it is also observed experimentally and numerically by previous research that the tip leakage vortex cavitation can induce negative $\Delta\alpha$ on the following blade (Kang et al., 2009; Kim and Song, 2019). The present analysis further supports the experimental results that no other local instabilities are observed at two-bladed inducer.

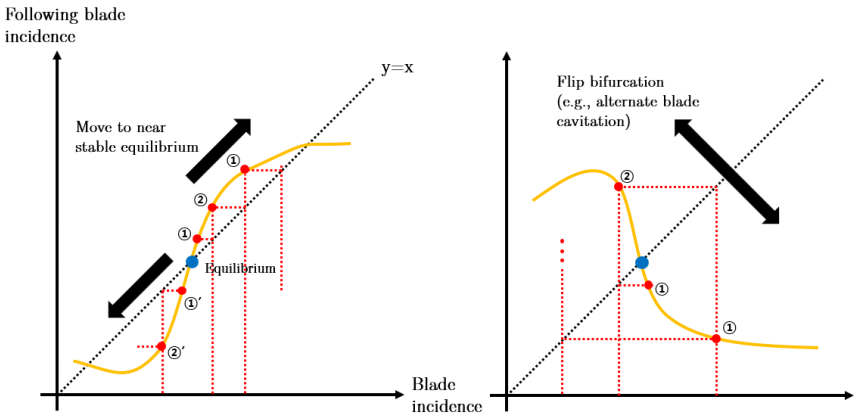

Figure 4 Unstable Equilibrium of Two-Bladed System

APPLICATION ON THREE-BLADED IMPELLER

The matrix differential equation of the three-bladed impeller is expressed as follows:

$$\dot{X} = \begin{bmatrix} 0 & 1 & 0 & 0 & 0 & 0 \\ -1/a & -b/a & c/a & 0 & 0 & 0 \\ 0 & 0 & 0 & 1 & 0 & 0 \\ 0 & 0 & -1/a & -b/a & c/a & 0 \\ 0 & 0 & 0 & 0 & 0 & 1 \\ c/a & 0 & 0 & 0 & -1/a & -b/a \end{bmatrix} \mathrm{X}, \qquad (7)$$

where $\mathrm{X} = [\mathrm{x}_1\ \dot{x_1}\ \mathrm{x}_2\ \dot{x_2}\ x_3\ \dot{x_3}]^T$.

Therefore, the characteristic equation of the given matrix is obtained as Eq. (8).

$$\frac{(a\lambda^2+b\lambda+1)^3-c^3}{a^3} = 0 \qquad (8)$$

However, even though the analytical solution of the Eq. (8) can be obtained by solving three different quadratic equation, the exact formula gives less chance to interpret the system than the two-bladed system. Therefore, its analysis will be deferred to the chapter which explains the general behaviour of the N-bladed system. In the present chapter, numerical results are presented.

Fig. 5 shows the maximum real value among six eigenvalues in the case of $c = 1.3$. The imaginary value of the corresponding eigenvalue is not shown in the figure while the values are all zero for the given case. From the Fig. 5, it can be shown that, for all possible system, the maximum real value of the eigenvalue is larger than 0 with no imaginary part. Therefore, as in the two-bladed system, it can be concluded that if c is larger than 1, the solution for each blade diverges with the same direction (see left figure of Fig. 4) and will drift to the adjacent equilibrium. Also, it can be shown that if $0 < c < 1$, the maximum real eigenvalue is negative, and the solution will converge to the equilibrium. It should be noted, nevertheless, that there are few exceptions for some a and b, and it is dealt in the next chapter.

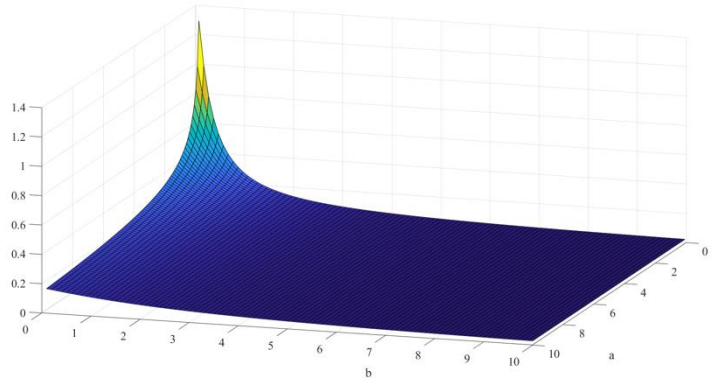

Figure 5 Maximum Real Eigenvalue of Three-Bladed System at c=1.3

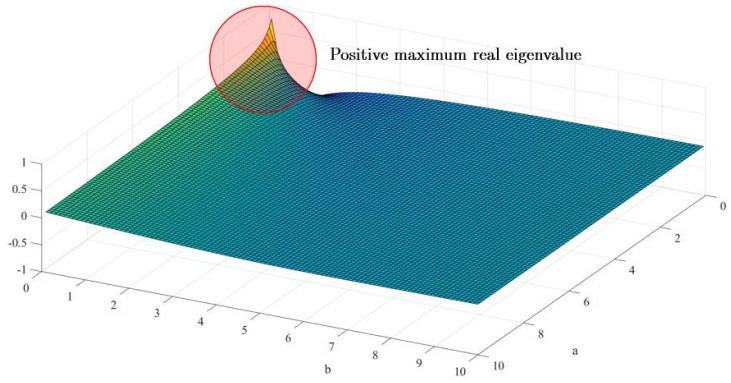

Figure 6 Maximum Real Eigenvalue of Three-Bladed System at c=-0.8

In the case which c is negative, two features different from the two-blade system appear. Fig. 6 shows the maximum real eigenvalue and Fig. 7 shows the imaginary part of the corresponding eigenvalue at $c = -0.8$. If a is significantly larger than b (large inertia and low damping for the blade dynamics), the equilibrium can be unstable even though the slope of the blade-to-blade interaction is larger than -1. Also, for all cases, the imaginary part of the eigenvalues is non-zero. Hence, the negative slope of the blade-to-blade interaction induces amplifying oscillation to the

three-bladed system. Fig. 8 shows the timewise evolution of the blades with small initial perturbation on the third blade from the equilibrium point. It can be shown from Fig. 8 that, by tracking the peak positions, the phase lag of the oscillation on each blade creates a pattern, seemingly propagates in the blade rotating direction (forward direction) in the order of blade 1, 3, and 2. This forward rotating local instability is often reported in the three-blade inducer as super-synchronous rotating cavitation (Tsujimoto et al., 1997). Therefore, the same negative slope blade-to-blade interaction in the cavitating inducer due to tip leakage vortex cavitation can cause alternate blade cavitation in the two-bladed inducer, and super-synchronous rotating cavitation in the three-bladed inducer.

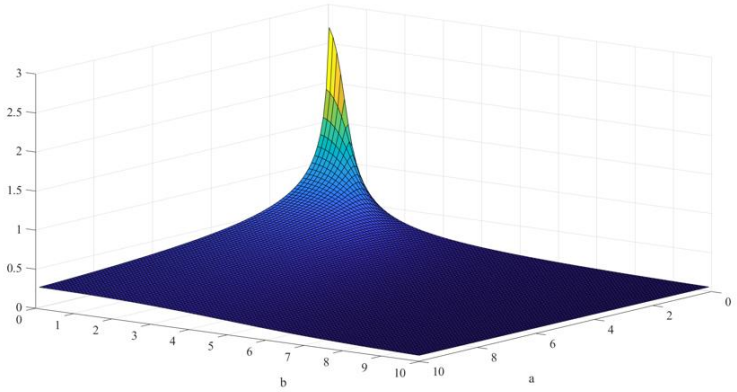

Figure 7 Imaginary Part of the Eigenvalue with Maximum Real Value at c=-0.8

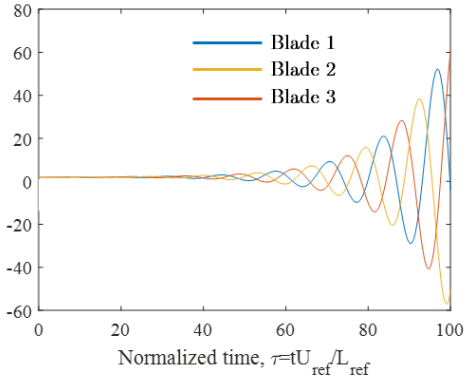

Figure 8 Timewise Evolution of the Three-Bladed Inducer at c=-0.8

GRAPHICAL ANALYSIS OF EIGENVALUES FOR GENERAL N-BLADED SYSTEM

For the general N-bladed system with N larger than 3, most of the system dynamics are the same with 2- and 3-bladed system. If c is negative and smaller than some critical number, it shows flip bifurcation as in 2-bladed system or forward-propagating local instability as in 3-bladed system. If c is negative but its absolute value does not exceed the critical number, the system is stable and remains at the equilibrium. For positive c, if c does not exceed 1, the system resides on the stable equilibrium, and if it exceeds 1, the system diverges unidirectional and moves to another equilibrium point (under actual non-linear blade-to-blade interaction). However, new local instability appears as N increases: backward-propagating local instability, whose structure is the same as compressor rotating stall. Fig. 9 shows the imaginary part of the maximum real eigenvalue for six-bladed inducer, $c = 1.3$. Even though the slope of the blade-to-blade interaction is the same with Fig. 5, for the large part of a and b, the imaginary part of the eigenvalue is non-zero, and the system diverges with oscillation. Fig. 10 shows the timewise progression of each blade of six-bladed impeller when $a = 3$, $b = 1$, and $c = 1.3$ with small initial perturbation of the sixth blade from equilibrium. In the same way as forward-propagating local instability in Fig. 8, the order of the peaks shows the local instability is propagating backward. In general, as N increases, the range of a and b increases which results in backward-propagating local instability, rather than unidirectional divergence for all blades. This phenomenon can be partially supported by the fact that in three-bladed inducer, some inducers show rapid increase of cavity length while the others rarely show sub-synchronous rotating cavitation in the same operating range, and almost all many-bladed rotors of compressor suffer from the rotating stall (Yoshida et al., 2007; Kikuta et al., 2008). To further investigate the characteristics of the eigenvalues for the N-bladed system, the following method is introduced.

The matrix differential equation of the general N-bladed system can equally be constructed as above, and the characteristic equation can also be obtained. The characteristic equation of the N-bladed system is as follows:

$$\frac{(a\lambda^2+b\lambda+1)^N-c^N}{a^N}=0 \qquad (9)$$

Therefore, the characteristic equation can be spilt into N different quadratic equations:

$$\begin{cases} a\lambda^2+b\lambda+1=c \\ a\lambda^2+b\lambda+1=ce^{\frac{2\pi}{N}i} \\ \vdots \\ a\lambda^2+b\lambda+1=ce^{\frac{2\pi}{N}(N-1)i} \end{cases} \qquad (10)$$

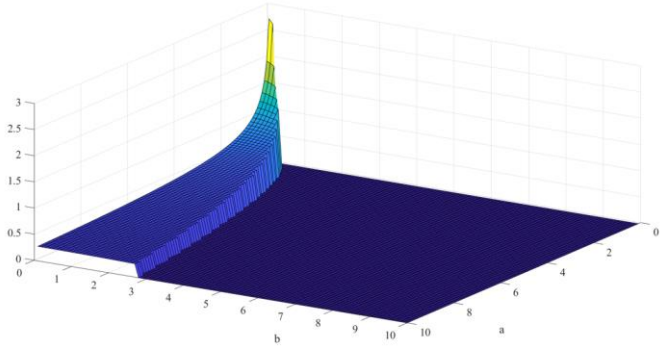

Figure 9 Imaginary Part of the Eigenvalue with Maximum Real Value for Six-Bladed Inducer at c=1.3

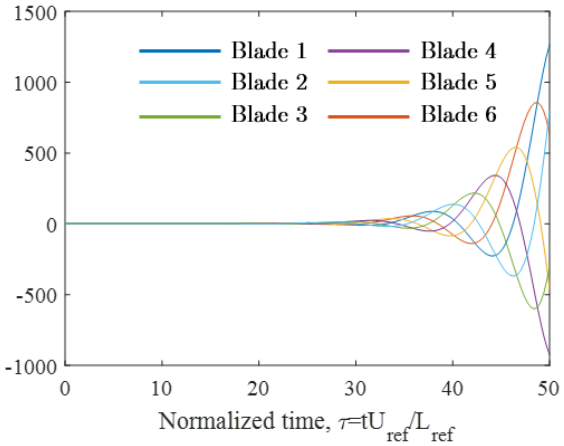

Figure 10 Timewise Evolution of the Six-Bladed Inducer at c=1.3

Thus, even though the slope of the blade-to-blade interaction, c, only varies among the real values, it would be mathematically useful to observe the solution of $a\lambda^2+b\lambda+1=c$ with $c\in\mathbb{C}$. In Fig. 11, the contour for the zero maximum real eigenvalue for complex c is drawn as a purple line for three sets of a and b. The right side of the contour is the positive real eigenvalue, and the left side is the negative real eigenvalue. Also shown as the yellow line is the contour for the maximum real eigenvalue of 0.2. It can be seen from the figure that increasing a will make the contour narrower and increasing b widen the contour. However, regardless of the values of a and b, the zero-eigenvalue contour always passes the point $c=1+0i$. It should be noted that, in the right side of the zero-eigenvalue contour, the only region that makes the imaginary part of the eigenvalue zero is the line $Im(c)=0$. Otherwise, the system will diverge with oscillation.

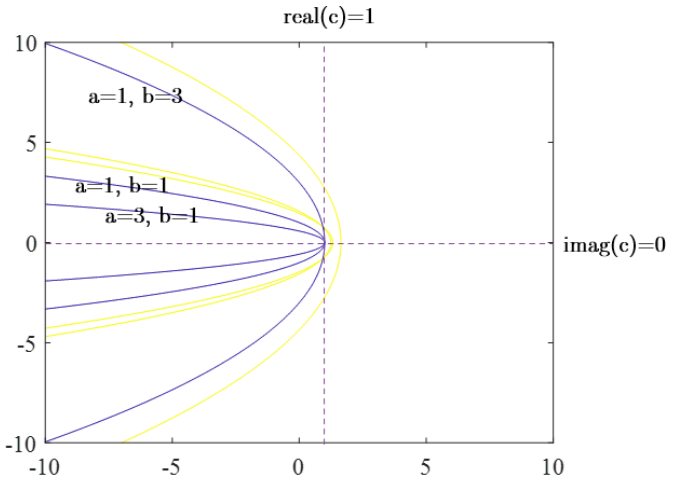

Figure 11 Zero Real Eigenvalue Contour

From Fig. 11, behaviour of the N-bladed system with varying a, b, and c can be graphically investigated. The left figure of the Fig. 12 shows the zero-eigenvalue contour for 2-bladed impeller. While the two-bladed system comprises two quadratic equations, $a\lambda^2 + b\lambda + 1 = c$ and $a\lambda^2 + b\lambda + 1 = -c$, the zero-eigenvalue contour in Fig. 11 is mirrored and overlapped. To make the equilibrium point stable, all the eigenvalues should have real value less than zero. Therefore, if c has value in the purple arrowed region, the system will be stable. For the two-bladed system, the intersections of zero-eigenvalue contour and the $Im(c) = 0$ are independent of the values of a and b, and fixed to $c = -1 + 0i$ and $c = 1 + 0i$. Thus, it can be shown that $|c| = 1$ is the criteria of stability in two-bladed system, as shown in the previous chapter.

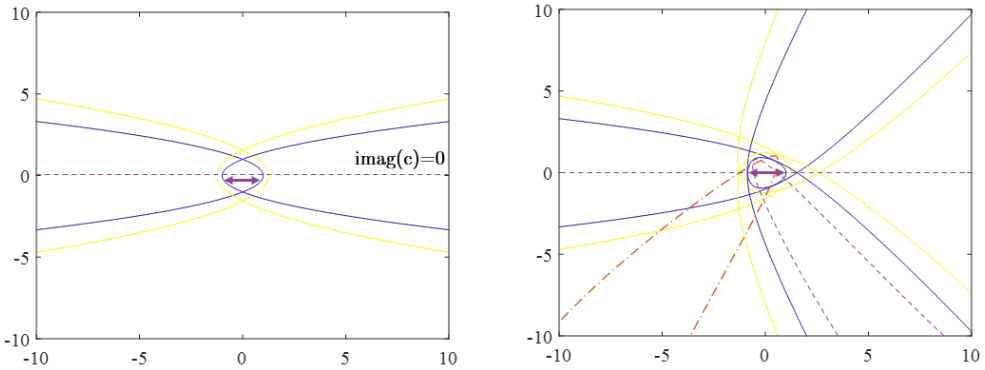

Figure 12 Zero Real Eigenvalue Contour for N-Bladed System

The three-bladed system can be also examined through the same method and its resulting zero-eigenvalue contour is shown in the right figure of Fig. 12. The contour consists of three zero-eigenvalue contours in Fig. 11, each was rotated with the angle of 0, $2\pi/3$, and $4\pi/3$. It can be shown from the intersections of the contours and the real axis that smaller absolute value of c can also induces unstable equilibrium. The contours of Fig. 11 are drawn based on the value $a = 1$ and $b = 1$. Consequently, the range of stable equilibrium is $-0.8 < c < 1.0$. However, by increasing a, the criterion of c value for stability, especially the upper bound, can be changed. For example, if the contour gets narrower as the bottom-right purple dashed line shows, the narrowed contour will intersect with the real axis at point smaller than the one due to the unrotated contour from Fig. 11. Therefore, the upper bound of the stability criterion will be reduced and the backward-propagating local instability is more easily produced. It should be noted that, while this upper bound is not restricted by the unrotated contour, the imaginary part of the maximum real eigenvalue is not zero and thus corresponds to the rotating local instability. Also, as N increases, similar effect can be observed. The red dot-dash line in Fig. 12 shows one of the extra overlapped contours if we increase N from 3 to 6. Although a and b are not changed, the upper bound of the stability criterion for c reduces and the system becomes more prone to the backward-propagating local instability. This explains the observation for many-bladed systems, which is shown at the first part of this chapter.

Even though the propagating direction of the instability is said to be determined by the sign of c, it has only been verified by previous experimental results and numerical simulations. Therefore, while the propagating direction is determined by the corresponding eigenvalue and eigenvector, present paper proposes a simple way to mathematically verify the relationship between propagating direction and the sign of c. Without loss of generality, assume the system is 3-bladed. Due to the real-valuedness of the system matrix in Eq. (7), eigenvalues and eigenvectors come in conjugate pairs. To make the system backward-propagating, the eigenvector which has the counter-clockwise order of the incidence of each blade, (x_1, x_2, x_3), should correspond to positive value of $\mathrm{Im}(\lambda)$ (the eigenvector with clockwise order of incidences needs not be examined considering that the eigenvectors appear as conjugate pairs). Conversely, forward-propagating system should correspond to negative value of $\mathrm{Im}(\lambda)$. If the system matrix is infinitely multiplied to an arbitrary counter-clockwise vector, the only eigenvalue with the largest $\mathrm{Re}(\lambda)$ will survive, and the sign of $\mathrm{Im}(\lambda)$ can be examined. However, in the same manner, only few times of multiplication also help to check the sign of $\mathrm{Im}(\lambda)$. If we multiply the system matrix twice to the simple counter-clockwise vector, $X_{cc} = [1\ 0\ \exp(i\,2/3\,\pi)\ \ 0\ \ \exp(i\,4/3\,\pi)\ \ 0]^T$, it becomes $X_{cc,t} - 1/a X_{cc} + c/a X_{cc}\exp(i2/3\pi)$ (shown in Fig. 13 as black dot). Thus, the vertex of $X_{cc,t}$ corresponding to the vertex (1,0) of X_{cc} is on 2nd quadrant if c is positive and on 3rd quadrant if c is negative. However, if the real part of the dominant eigenvalue is positive and $X_{cc,t}$ is on the 2nd quadrant, the imaginary part of the dominant eigenvalue should be positive (square root of the complex number on 2nd quadrant goes to the 1st quadrant). Also, if the $X_{cc,t}$ is on the 3rd quadrant, the imaginary part of the dominant eigenvalue should be negative (square root of the complex number on 3rd quadrant goes to 4th quadrant). From those observation, it can be said that the sign of c determines the propagating direction of the instability as mentioned above, at least if the instability tends to diverge. While the diverging instabilities with $\mathrm{Re}(\lambda) > 0$ is concerned in most cases, it can be safely said that the positive slope of blade-to-blade interaction results in backward propagating instability and the negative slope induces forward propagating instability.

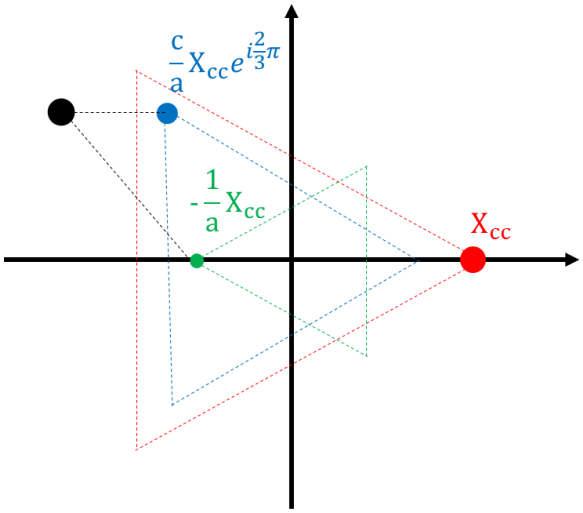

Figure 13 Transformed Counter-Clockwise Eigenvector

SUMMARY AND CONCLUSIONS

In the present study, a new approach has been proposed which concerns the stability and types of instability of the N-bladed system by simplified model of blade itself and blade-to-blade interaction. Through linearization of the blade-to-blade interaction and following eigenvalue analysis of the system, two- and three-bladed system are examined and their correspondence with the previous experimental results are established. Also, a graphical approach for the general N-bladed system is given, and the qualitative behaviour of the system eigenvalues are explained. By obtaining the non-linear blade-to-blade interaction and determining the blade modelling parameters, such as a and b, experimentally, the present method can be extended to identify and estimate the local instability for the N-bladed turbomachines.

ACKNOWLEDGMENTS

This work was supported by BK21+ Program and Seoul National University Institute of Advanced Machines and Design (SNU-IAMD).

REFERENCES

Hewkin-Smith, M., Pullan, G., Grimshaw, S. D., Greitzer, E. M. and Spakovszky, Z. S. (2019). The Role of Tip Leakage Flow in Spike-Type Rotating Stall Inception. *ASME Journal of Turbomahicnery*, 141(6), pp. 061010.

Horiguchi, H., Watanabe, S. and Tsujimoto, Y. (2000). A Linear Stability Analysis of Cavitation in a Finite Blade Count Impeller. *ASME Journal of Fluids Engineering*, 122(4), pp. 798-805.

Huang, J.-D., Aoki, M. and Zhang, J.-T. (1998). Alternate Blade Cavitation on Inducer. *JSME International Journal Series B Fluids and Thermal Engineering*, 41(1), pp. 1-6.

Kang, D., Yonezawa, K., Horiguchi, H., Kawata, Y. and Tsujimoto, Y. (2009). Cause of Cavitation Instabilities in Three Dimensional Inducer. *International Journal of Fluid Machinery and Systems*, 2(3), pp. 206-214.

Kikuta, K., Yoshida, Y., Watanabe, M., Hashimoto, T., Nagaura, K. and Ohira, K. (2008). Thermodynamic Effect on Cavitation Performance and Cavitation Instabilities in an Inducer. *ASME Journal of Fluids Engineering*, 130(11), pp. 111302.

Kim, J. and Song, S. J. (2019), Visualization of Rotating Cavitation Oscillation Mechanism in a Turbopump Inducer. *ASME Journal of Fluids Engineering*, 141(9), pp. 091103.

Moore, F. K. and Greitzer, E. M. (1986). A Theory of Post-Stall Transients in Axial Compression Systems: Part I—Development of Equations. *ASME Journal of Engineering for Gas Turbines and Power*, 108(1), pp. 68-76.

Murayama, M., Yoshida, Y. and Tsujimoto, Y. (2006). Unsteady Tip Leakage Vortex Cavitation Originating from the Tip Clearance of an Oscillating Hydrofoil. *ASME Journal of Fluids Engineering*, 128(3), pp. 421-429.

Semenov, Y. and Tsujimoto, Y. (2003). A Cavity Wake Model Based on the Viscous/Inviscid Interaction Approach and Its Application to Nonsymmetic Cavity Flows in Inducers. *ASME Journal of Fluids Engineering*, 125(5), pp. 758-766.

Tsujimoto, Y., Kamijo, K. and Brennen, C. E. (2001). Unified Treatment of Flow Instabilities of Turbomachines. *AIAA Journal of Propulsion and Power*, 17(3), pp. 636-643.

Tsujimoto, Y., Kamijo, K. and Yoshida, Y. (1993). A Theoretical Analysis of Rotating Cavitation in Inducers. *ASME Journal of Fluids Engineering*, 115(1), pp. 135-141.

Tsujimoto, Y., Yoshida, Y., Maekawa, Y., Watanabe, S. and Hashimoto, T. (1997). Observations of Oscillating Cavitation of an Inducer. *ASME Journal of Fluids Engineering*, 119(4), pp. 775-781.

Vo, H. D., Tan, C. S. and Greitzer, E. M. (2008). Criteria for Spike Initiated Rotating stall. *ASME Journal of Turbomachinery*, 130(1), pp. 011023.

Von Kárman, T. and Sears, W. R. (1938). Airfoil Theory for Non-Uniform Motion. *Journal of the Aeronautical Sciences*, 5(10), pp. 379-390.

Watanabe, S., Sato, K., Tsujimoto, Y. and Kamijo, K. (1999). Analysis of Rotating Cavitation in a Finite Pitch Cascade Using a Closed Cavity Model and a Singularity Method. *ASME Journal of Fluids Engineering*, 121(4), pp. 834-840.

Xu, D., Dong, X., Zhou, C., Sun, D., Gui, X. and Sun, X. (2021). Effect of Rotor Axial Blade Loading Distribution on Compressor Stability. *Aerospace Science and Technology*, 119, pp. 107230.

Yoshida, Y., Sasao, Y., Okita, K., Hasegawa, S., Shimagaki, M. and Ikohagi, T. (2007). Influence of Thermodynamic Effect on Synchronous Rotating Cavitation. *ASME Journal of Fluids Engineering*, 129(7), pp. 871-876.